# Stereoscopic PIV measurements in a two-stage axial turbine

*Luca* Porreca[1*], *Anestis I.* Kalfas[2†], *Reza S.* Abhari[1‡], *Yong Il* Yun[3§], and *Seung Jin* Song[3**]

[1]ETH, Swiss Federal Institute of Technology, Turbomachinery Laboratory, Zurich, Switzerland
[2]AUTh, Department of Mechanical Engineering, Laboratory of Fluid Mechanics and Turbomachinery, Thessaloniki, Greece
[3]Seoul National University, School of Mechanical and Aerospace Engineering, Seoul, Korea

**Abstract.** In the present work, the three-dimensional flow field in the interstage region of a twostage axial turbine has been measured by a stereoscopic PIV system. The stereoscopic method is used to compensate for perspective as well as to observe the highly threedimensional flows. The digital images are recorded with a set of two cameras positioned perpendicularly to the measurement plane and inclined by an angle varying between 22° and 30° to allow stereoscopic measurements. The laser beam is delivered to a laser endoscope able to access the measurement areas. By traversing radially, several blade-to-blade planes can be illuminated with the laser endoscope from 66 to 96% blade span. To compensate for the perspective distortion of the field of view due to the tilt angle of camera B as well as the optical distortion through the double-curvature windows, a threedimensional calibration method is used. In the current investigation, a Monte Carlo simulation has been conducted to evaluate measurement errors of PIV. Results of these measurements are compared with velocities derived from time resolved pressure measurements using fast aerodynamic response probe (FRAP). A good agreement is found at the exit of the second rotor. The present work present a unique set of steady and unsteady data measured in a two-stage axial turbine. Measured data in a volume can be used for numerical tool validation as well as improve existing kinematic model of vortex transport and dissipation.

## 1 Introduction

The flow field in a turbomachine is always unsteady and three dimensional. Common reasons to generate such a flow are the presence of secondary flows near the endwall, radial migration of wake fluids and effect of leakages from the hub and the tip blades. Evolution of these flow features in an axial turbomachine is of great importance to define loss generation and improve aerodynamic performances.

In order to gain understanding in flow physics and improve airfoil design procedures, measurements using miniaturize steady (pneumatic) and unsteady probes have been always of prime interest for designers. Measurements with multi-holes pneumatic probes are common in several applications. In particular, 5-Hole probe pneumatic technology is currently considered as the most reliable for performance evaluation and reaches nowadays the complete development.

Recently, unsteady phenomena have received more and more attention in the design process and different experimental techniques have been developed able to capture unsteady flow field such as fast response aerodynamic probes. Beside probe technology, optical measurements techniques such as Particle Image Velocimetry (PIV) have been applied more and more to rotating machinery. However this technique is still a challenge in such an environment because of the difficult optical access and the need to use a uniquely defined calibration procedure to take into account the image distortion due to the cylindrical shape of the window. Moreover, since PIV measures the velocity field of tracers that are added to the flow, achieving a uniform seeding with an optimum concentration is crucial. In large scale, rotating turbomachinery research facilities, these issues are very critical.

For these reasons, there are only a few publications of the successful application of PIV to turbomachinery. Wernet [1], Balzani et al. [2], Sanders et al. [3] and Uzol et al. [4] studied the 2D steady and transient flow field in axial and centrifugal compressors. Göttlich et al. [5] and Liu et al. [6] made stereoscopic PIV measurements focusing on the wake-wake interaction at midspan in an axial transonic turbine and in the tip region of an axial compressor respectively.

* *Luca* Porreca: Luca.Porreca@ch.manturbo.com
† *Anestis I.* Kalfas: akalfas@auth.gr
‡ *Reza S.* Abhari: abhari@lec.mavt.ethz.ch
§ *Yong Il* Yun: yongil.yun@samsung.com
** *Seung Jin* Song: sjsong@snu.ac.kr

In the present work, extensive measurements Stereoscopic PIV are made in a two-stage shrouded axial turbine.

## 2 Measurement principle

Tracer particles are added to the flow and illuminated twice by a double-pulsed laser light sheet. The light scattered by the particles is recorded by means of CCD cameras synchronized with the laser pulsations. The particle displacement can thus be determined by comparing the two recorder images. The velocity filed can be obtained by dividing the particle displacement by the time interval between the two laser pulses. The velocity vectors are derived from sub-sections of the target area of the particle-seeded flow by measuring the movement of particles between two light pulses. The camera lens images the target area onto the CCD array of a digital camera. The CCD is able to capture each light pulse in separate image frames. Once a sequence of two light pulses is recorded, the images are divided into small subsections called inter-rogation areas. The interrogation areas from each image frame are cross-correlated with each other, pixel by pixel. The correlation produces a signal peak, identifying the common particle displacement. A velocity vector map over the whole target area is obtained by repeating the cross-correlation for each interrogation area over the two image frames captured by the CCD camera.

### 2.1 Illumination system

A double-cavity Nd:YAG laser provided by New Wave Research Ltd is used as a light source. The laser generates a maximum of 120 mJ/pulse of 532 nm wavelength green visible light that, corresponds to a power of almost 120 MW at each pulse width of 10 ns. The maximum pulse repetition rate is 15 Hz. The bursts of laser light are synchronized with cameras via a Dantec FlowMap system hub. The laser beam is delivered to a laser endoscope (ILA Intelligent Laser Applications) through an articulated mirror arm. The laser endoscope not only generates laser sheet through a cylindrical lens but also bends the laser sheet by 90° with a prism at the tip. The outer diameter of the laser endoscope is 8 mm and the divergence angle of the laser sheet is approximately 16°.

### 2.2 Camera set up

The stereoscopic PIV system has been installed in the LISA axial turbine facility. The cameras, the laser light source and the endoscope have been installed in the traversing system of the turbine rig. The whole arrangement can be traversed in the circumferential direction. Moreover, the cameras and laser endoscope are also mounted on a motor-controlled 1-axis linear stage so that cameras and the light sheet move together in the radial direction (Figure 1). The digital images are recorded with 1280x1024-pixel 12-bit CCD cameras (PCO SensiCam SVGA) whose pixel size and pitch are 6.7x6.7 µm and 9 µm, respectively. The cameras are set taking into account the Scheimpflug condition (Zang and Prasad [7]). A standard Nikon AF MICRO NIKKOR lenses with a focal length of 60 mm are used for camera optics. By traversing radially the entire system, several blade-to-blade planes can be illuminated with a laser endoscope. Camera A is positioned such that its axis is perpendicular to the light sheet plane to avoid an interference with the laser endoscope. Camera B is tilted by different angles (22°, 25°, 30°) as shown in Figure 1.

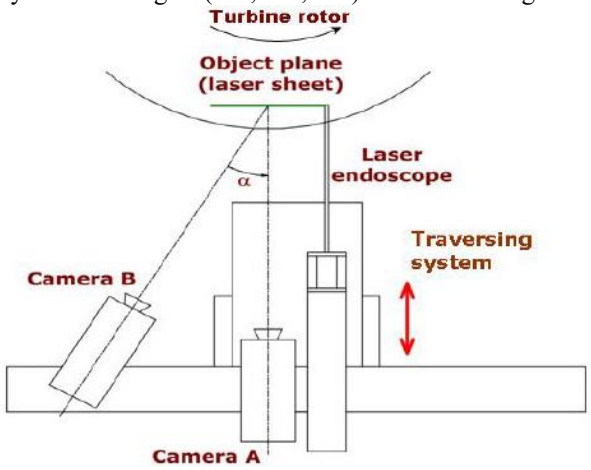


**Fig. 1.** Stereoscopic camera configuration in test turbine

The image plane (CCD plane) of camera B is further rotated by 5° to satisfy the Scheimpflug condition which ensures that all particles in the object field will be in good focus in the image plane (Prasad [8]).

Two optical windows made of acrylic PMMA are installed in the test turbine. The window surface has been carefully polished to achieve good transparency and they have a thickness of approximately 2 mm. A FEM analysis has been conducted in order to ensure that mechanical stresses due to the pressure field of the turbine casing are within the security margin of the material. The windows are located between the first rotor and the second stator (interstage area) as well as downstream of the second rotor (downstream area). The windows are designed to reproduce the exact shape of the double curvature contoured casing inner wall.

### 2.3 Seeding

In the PIV technique, the velocity measurements are based on the scattering of the light by particles suspended in the flow. Therefore achieving a good quality of seeding is a critical issue in the measurement chain. Particle should be small enough to follow the flow as close as possible and sufficiently large to scatter properly the laser light. Moreover, the seeding should not be toxic sand corrosive since the LISA test facility is open to the atmosphere. Oil DEHS ($C_{26}H_{50}O_4$) was chosen to seed the flow into the turbine. It is enough volatile to recirculate partly in the turbine loop and, unlike other seeding oils, it completely evaporate after 4 hours avoiding high contamination of the environment close to the turbine rig. Particle of DEHS are still detectable at a temperature up to 120°. The seeding was achieved using a commercial laskin [9] nozzle manufactured by PIVTEC. The nominal particle diameter was 1 µm which is considered as

adequate[10] for a frequency response up to 10 kHz. To obtain a uniform concentration an injection device was designed to seed the entire air mass flow. Thus a global seeding can be achieved ensuring the lowest level of disturbances of the flow by the measurement techniques. The seeding injection has been placed downstream the radial compressor and upstream the inlet flow conditioning stretch. Deposits of seeding material on the casing windows were not significant during the operation.

## 2.4 Measurement areas and data post processing

Figure 2 shows the measurement planes of FRAP and 5HP probe and the PIV region at the interstage and at the turbine exit region. The first stator is not shown in the figure for a better visualization of the measurement areas. Regarding the interstage region, measurements were taken in 15 blade-to-blade planes from 66 to 97 percent span. One blade passing period is divided into 20 time steps, and between 60 and 100 digital image pairs for each measurement plane at each time step are recorded of a 50x40 $mm^2$ area in the flow.

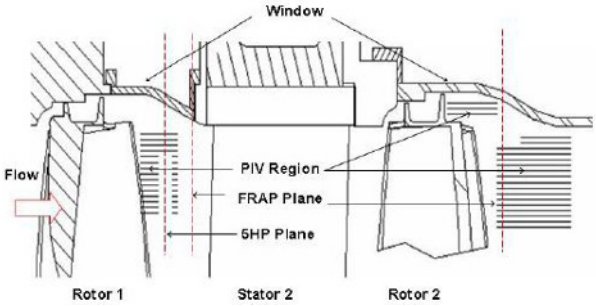


**Fig. 2.** Measurement regions: PIV, FRAP and 5HP planes

For the downstream region, measurements are done on 3 planes inside the shroud cavity and 17 blade-to-blade planes (from 60 to 96 percent span) downstream of the second rotor. One blade passing period is divided into 10 time steps, and 100 image pairs are recorded on each plane at each time step.

In the interstage area, the region of the window with abrupt change of curvature provides a severe optical distortion that could not be corrected by the calibration procedure. Therefore, data measured in this region have been blanked. The time interval between two bursts varies between 2 and 4 μs depending on the average flow field velocity. Each pair of images is interrogated using cross-correlation analysis in 32x32-pixel sub-images with an overlap of 50 percent between adjacent interrogations. An advanced interrogation method of window offset [11,12] is used. The theoretical analysis and simulations performed by Westerweel et al. [11] show that the signal-to-noise ratio with window offset is approximately three times larger than that without window offset for flow with high turbulence intensity. Furthermore, the method of window offset is effective to reduce the error due to loss-of-pairs. To filter out spurious data, the local median is used [13]. Figure 3 shows a recorded image in the interstage measurement region. Visible in the picture are the blade trailing edge, the shroud platform, and the seeding illuminated by the laser beam.

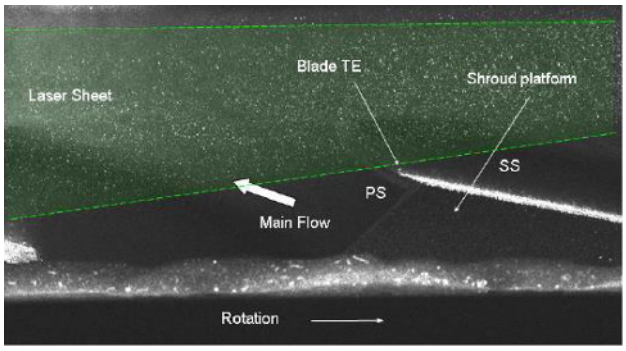


**Fig. 3.** Recorded image of seeded flow in the interstage region

## 2.5 Calibration procedure

To compensate for the perspective distortion of the field of view due to the tilted angle of camera B as well as optical distortion through the double-curvature windows, a three-dimensional calibration method is used. Although an in-situ calibration is often used in stereoscopic PIV measurements, the complexity of the geometry inside a turbomachinery could not allow to apply this procedure. A separate test bench shown in Figure 5 has been designed where the stereoscopic calibration procedure is applied. The calibration bench is reproducing exactly the same test section and optical access of the turbine. The same relative position and arrangement between calibration target and cameras are then applied on the turbine rig.

Calibration target is designed following the guidelines of Dantec Dynamics. It is composed by a grid of circular markers with diameter of 0.8 mm and uniform spacing of 2.4 mm. Figure 4 shows the calibration target acquired by camera A and B. Calibration target could be traversed in radial direction by using a 1dimensional linear manual traversing system. Each measurement plane (15 in the interstage region, 17 in the downstream region) has been calibrated using the calibration bench to take into account the same optical distortion caused by the curved window. The locations of the calibration markers have been recorded at three different out-of-plane locations spacing between -0.5 mm, 0 and +0.5 mm at each radial location. This displacement was selected taking into account that the approximate laser light thickness is 1 mm.

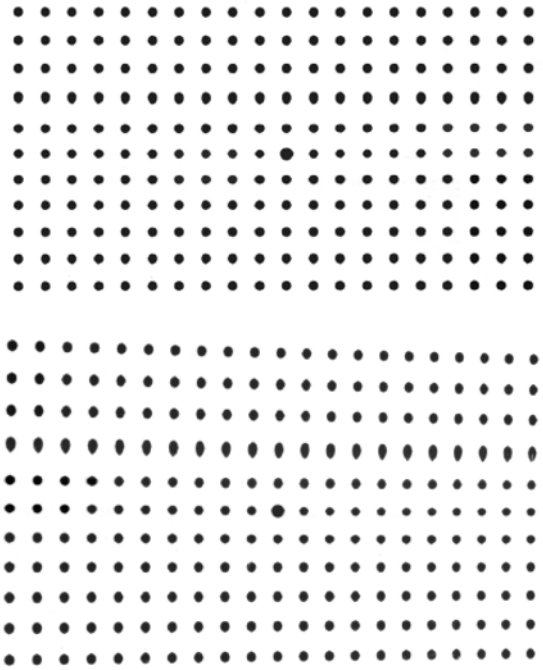

**Fig. 4.** Recorded calibration target in plane 2 a) camera A b) camera b

Images of the calibration target were acquired by both cameras. An algorithm has been programmed in order to achieve a polynomial fitting between the original calibration target markers and the distorted picture. The variation of the location of each marker points in the out-of-plane direction can be considered as linear in a range of +/- 0.5 mm, thus a quadratic polynomial function is sufficient. However, in the circumferential and axial direction (in-plane velocity components) both perspective and window optical distortion are highly non liner. Therefore a 7$^{th}$ order polynomial function has been used. Residual values are calculated to assess the magnitude of the calibration procedure at each plane.

**Table 1.** Calibration RMS residual values for measurement plane at the interstage region

| Cal # | Cam. A (pix) | Cam. B (pix) | PO | | | |
|---|---|---|---|---|---|---|
| 1 | 0.76 | 0.70 | 7 | | | |
| 2 | 2.38 | 2.53 | 7 | | | |
| 3 | 2.63 | 2.79 | 7 | | | |
| 4 | 2.81 | 2.90 | 7 | | | |
| 5 | 2.92 | 2.93 | 7 | | | |
| | **Cam. A-L (pix)** | **Cam. B-L (pix)** | **PO - L** | **Cam. A-U (pix)** | **Cam. B-U (pix)** | **PO-U** |
| 6 | 0.321 | 0.393 | 6 | 0.295 | 0.366 | 3 |
| 7 | 0.315 | 0.362 | 6 | 0.294 | 0.351 | 3 |
| 8 | 0.318 | 0.380 | 6 | 0.275 | 0.359 | 3 |
| 9 | 0.331 | 0.434 | 6 | 0.281 | 0.370 | 3 |
| 10 | 0.346 | 0.449 | 6 | 0.273 | 0.405 | 3 |
| 11 | 0.363 | 0.493 | 6 | 0.269 | 0.408 | 3 |
| 12 | 0.380 | 0.536 | 6 | 0.275 | 0.416 | 3 |
| 13 | 0.407 | 0.575 | 6 | 0.292 | 0.442 | 3 |
| 14 | 0.420 | 0.621 | 6 | 0.299 | 0.457 | 3 |
| 15 | 0.426 | 0.646 | 6 | 0.310 | 0.481 | 3 |
| 16 | 0.440 | 0.670 | 6 | 0.321 | 0.428 | 3 |

Table 1 shows the residuals obtained in each planes at the interstage region. Magnification factor in this case is equal to 4.34 resulting from a measurement length of 50 mm for a corresponding length of the CCD plane of 11.52 mm. In this case, one pixel corresponds to 9e-3 mm and therefore the maximum error occurring in the polynomial reconstruction procedure (2.93 pixel in plane N.5) is equal to 0.026 mm or 0.05% with respect to the rotor blade axial chord. Thus it can be considered as negligible. With the described procedure, nominal particle displacements can be calculated for both cameras using the calibration coefficients. Once the overlapped region has been defined one can evaluate the displacement vector using the displacements seen from both cameras as:

$$\begin{bmatrix} \Delta x_1 \\ \Delta y_1 \\ \Delta x_2 \\ \Delta y_2 \end{bmatrix} = \begin{bmatrix} F_{11}^A & F_{12}^A & F_{13}^A \\ F_{21}^A & F_{22}^A & F_{23}^A \\ F_{11}^B & F_{12}^B & F_{13}^B \\ F_{21}^B & F_{22}^B & F_{23}^B \end{bmatrix} \cdot \begin{bmatrix} \Delta x_1 \\ \Delta x_2 \\ \Delta x_3 \end{bmatrix} \quad (1)$$

Where the LHS represents the nominal displacement seen by both cameras. The RHS matrix is knows from the calibration procedure, thus the true displacement ($\Delta x_1$, $\Delta x_2$, $\Delta x_3$) can be evaluated using a least square method.

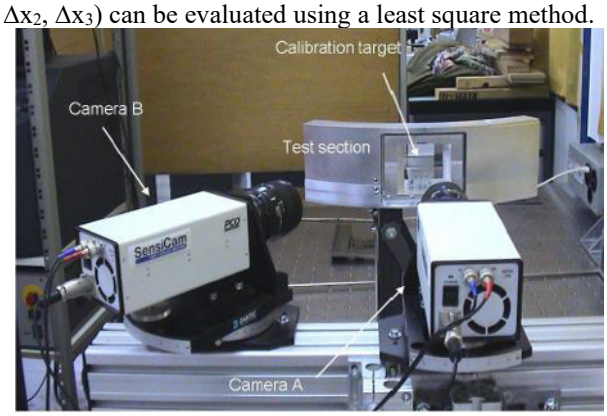


**Fig. 5.** Stereoscopic PIV calibration test bench

## 2.6 Uncertainty analysis

For the estimation of the uncertainty in the PIV velocity measurements many parameters have to be considered (Raffel et al. [14] Willert and Gharib [15]).These include:

- particle image diameter; - displacement of the particle relative to the size of the interrogation area size; - particle image density;
- local velocity gradients; - out-of-plane motion of tracer particles; and
- background noise.

There is no established method to analytically evaluate the uncertainty in PIV measurements due to the above factors. Therefore, the assessment of PIV accuracy may be done for each PIV system by using one of the following three methods. The first method is to make PIV measurements in a flow field with an exact solution (e.g. Poiseuille flow or three-dimensional rotating disk flow) and then evaluate uncertainty for the flow field. However, it is difficult to guarantee that the uncertainty determined in a canonical flow field can be applied to other more general flow fields. Also, it is not always possible to introduce such canonical flows with exact solutions in a specific environment such as the current test rig. The second method is to conduct a

Monte Carlo simulation of particle displacements [14,16]. This approach allows the uncertainty of PIV measurements in a broad range of flow fields to be assessed. Third, PIV results can be compared against data obtained with hot wire or pneumatic probe methods or from direct numerical simulation [12]. However, a rigorous evaluation of uncertainty is difficult with this method, since the measurement techniques are different and the direct numerical simulation itself has uncertainties.

In the current investigation, a Monte Carlo simulation has been conducted to evaluate measurement errors of PIV. To carry out a Monte Carlo simulation, tracer particle images must be artificially generated. The light intensity scattered from individual tracer particles is assumed to have a Gaussian profile in both the in-plane ($x$, $y$) and out-of-plane ($z$) directions:

$$I(x,y,z) = I_0 exp\left[\frac{-(x-x_0)^2-(y-y_0)^2}{(1/8)d^2}\right]\exp\left[-\frac{z_0^2}{(1/8)\Delta z_0^2}\right] \quad (2)$$

The location of each tracer particle ($x_0$, $y_0$, $z_0$) is set by using a random number generator. Then, the light intensity scattered from the particle at each location in an interrogation area can be defined from Eq. (1).

Four parameters – particle image diameter, number of particles, maximum light intensity $I_0$ and actual displacement – must be given a priori. The diameter of tracer particles is set such that the particle fills a 2×2 pixel or 3×3 pixel region. The number of particles used here is 50. Both of these parameters were determined via a trial-and-error process so that the artificially generated images look similar to the measured images. Based on these artificial images, the first and second image frames with a time interval between 2 and 4μs can be generated. The actual displacements of the particle ($\Delta x, \Delta y, \Delta z$) are taken from a representative averaged velocity value measured with PIV at each point of interest.

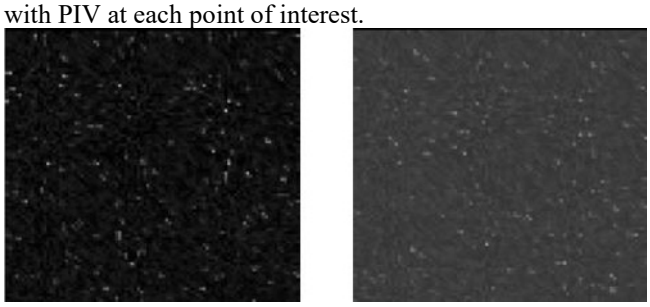

**Fig. 6.** Actual particle image (left) and artificially generated image (right) for the uncertainty analysis

Based on these displacements, the image pairs of tracer particles in the object plane can be generated.
The images are not generated for the entire field of view (for the current investigation, 50×40 mm) but at three points (as shown in Table 2). A point in the field of view corresponds to a 32×32 pixel interrogation window in the image plane. However, the images are generated in a 96×96 pixel region to properly account for the particles that enter and exit the 32×32 pixel interrogation area that is located at the center of the 96×96 pixel region. With stereoscopic PIV, the displacement values seen by the two cameras are different, particularly when there are out-of-plane displacement components. Also, perspective and optical distortions of the images occur when the particle images are projected onto the image planes. The calibration procedure is used to estimate both the image distortion and the displacements seen in both cameras' image planes. The interrogation area is also subject to background noise due to reflection on solid surfaces and the light that is scattered from tracer particles located outside the light sheet. Therefore, the background noise has a static intensity level (from the reflection) as well as a randomly moving pattern (from the scattering of particles outside the light sheet). To obtain a spatially random intensity pattern, a random number generator has been used. Then, the background noise is superimposed on the particle images. Because there is a randomly moving pattern in the background, the noise patterns for the first and the second frames are separately generated. 300 particle image pairs for each point are generated to carry out statistical evaluations. The stereoscopic PIV error is then evaluated comparing the imposed displacements to the displacements calculated from the artificially generated images. The measurement error consists of two parts, *bias error* and *root-mean-square* (*rms*) *error* [14].

$$\varepsilon_{PIV} = \varepsilon_{bias} + \varepsilon_{rms} \quad (3)$$

The bias error is defined as the difference between the actual velocity value and the averaged value measured with PIV. This bias error originates from loss-of-pairs and velocity gradients in the interrogation areas.
Rms error is the standard deviation of the values measured with PIV and can be regarded as measurement uncertainty of PIV. Table 2 shows results of the uncertainty analysis expressed in terms of the bias and rms error at the interstage and turbine regions. The bias error at the interstage region for the axial and tangential velocity (in-plane components with respect to the laser light sheet) is always in the range of ±2 m/s.

**Table 2.** Uncertainty analysis of stereoscopic PIV measurements

Interstage Region

| | | Velocity [m/s] | | | |
|---|---|---|---|---|---|
| *Span* | | *Tang. Velocity* | *Axial Velocity* | *Radial Velocity* | *Yaw Angle [°]* |
| *96%* | Actual values | **30** | **-5** | **10** | **80.54** |
| | Mean | 28.31 | -3.91 | 8.31 | 82.16 |
| | St deviation | 3.09 % | 14.23 % | 24.72 % | 1.62 % |
| | Bias Error [m/s] | **1.7** | **-1.09** | **1.7** | **-1.63** |
| *66%* | Actual values | **30** | **65** | **10** | **24.7** |
| | Mean | 28.32 | 62.99 | 16.59 | 24.22 |
| | St deviation | 7.53 % | 4.15 % | 50.97 % | 7.80 % |
| | Bias Error [m/s] | **1.68** | **2.01** | **-6.59** | **0.55** |

Turbine exit region

| | | Velocity [m/s] | | | |
|---|---|---|---|---|---|
| *Span* | | *Tang. Velocity* | *Axial Velocity* | *Radial Velocity* | *Yaw Angle [°]* |
| *85%* | Actual values | 10 | 30 | 5 | 18.43 |
| | Mean | 13.09 | 31.10 | 1.08 | 22.83 |
| | St deviation | 19.9 % | 11.6 % | 11.88 % | 18.0 % |
| | Bias Error [m/s] | **3.09** | **1.10** | **-3.92** | **4.40** |

Standard deviation is in the range of 4-7% at the lower span and higher close to the tip where the absolute velocity magnitude is smaller. In the turbine exit region, the magnitudes of the bias errors are similar, but the *rms* errors are larger.

The bias error of the radial velocity (out-of-plane component) is more than 10% in all the planes, therefore, the radial velocity measurements ought to be assessed only qualitatively. Another trend is that the errors of the in-plane components (tangential and axial velocities) are similar for all three locations while the error of the out-of-plane component increases as the measurement location is farther from the optical window. Measurement planes farther from the window suffer from more severe optical distortion. Thus, the error of the out-of-plane component appears to be more susceptible to optical distortion.

## 2.7 FRAP-3DPIV comparison

Figure 7a,b shows a comparison between the velocity measured by the 3D PIV technique (a) and the FRAP data (b). FRAP data are presented in the same domain than the PIV measured region. Regions with insufficient laser illumination are blanked at the left and right borders. Both pictures are presented with the same scale and levels. The higher tangential velocity region on the middle of the pictures shows the presence of the tip passage vortex occurring between 0.8 and 0.9 span height. The comparison shows a good agreement between the two measurement techniques. In the PIV plot, the high tangential velocity core is slightly larger with respect to the FRAP measurements, however location of the vortex and absolute the core middle, differences are limited in the range of +/- 1.5 m/s that is in agreement with the uncertainty detected in the PIV measurements shown in the previous section.

Figure 7c shows the relative total pressure coefficient measured by the FRAP probe at the same blade position. Corresponding with the underturning flow region, a local relative total pressure reduction is measured. Figure 8a shows the pitchwise yaw angle on different axial planes downstream the second rotor blade. The time averaged FRAP and PIV data are presented together with 5-Hole-Probe measurements. Because of blanked regions on the PIV set at the FRAP and 5HP measurement plane (153% tip axial chord) the data are presented on planes farther downstream starting form 171% to 208% distance.

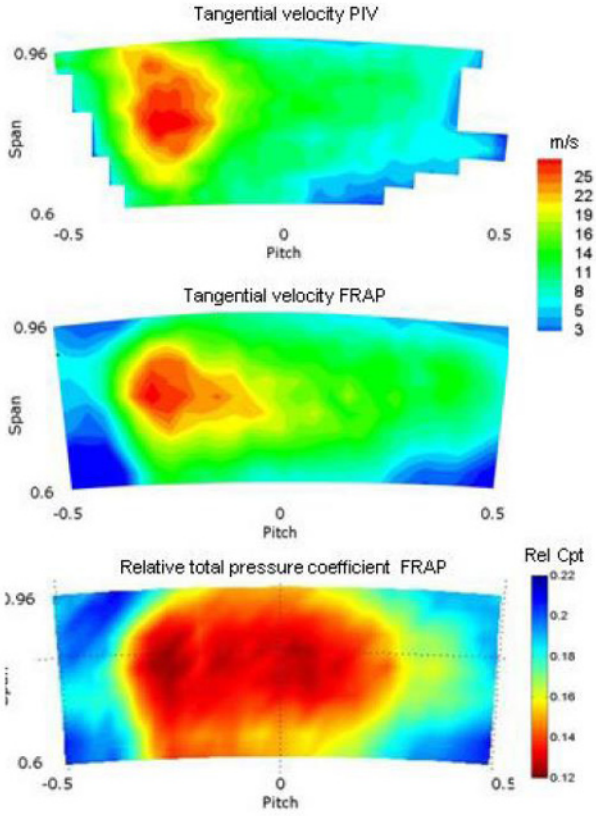


**Fig. 7.** Measured tangential velocity downstream turbine region a) PIV b) FRAP c) Relative total pressure coefficient

A good agreement again is observed between the probe and the optical measurement techniques. Underturning – overturning behavior is observed from 0.7 span up to the blade tip where the design intention is to align the flow with the underturned leakage flow in order to minimize mixing losses. Yaw angle profile measured by the probes (FRAP and 5HP) lays on the same line up to 0.75 span, then small discrepancies of about +/- 1.5° are observed up to the blade tip. Due to the high unsteadiness generated by the passage vortex in this region the time averaged signal of a fast response probe does not necessarily coincide with the pneumatic average of the 5HP. The PIV time averaged data are in good agreement with the probe data. Differences are of the order of +/- 2.5° in the region up to 0.9 blade span. Above 90% span, in the area of overturning due to the leakage layer, the trend is captured correctly but higher differences with probe data are detected.

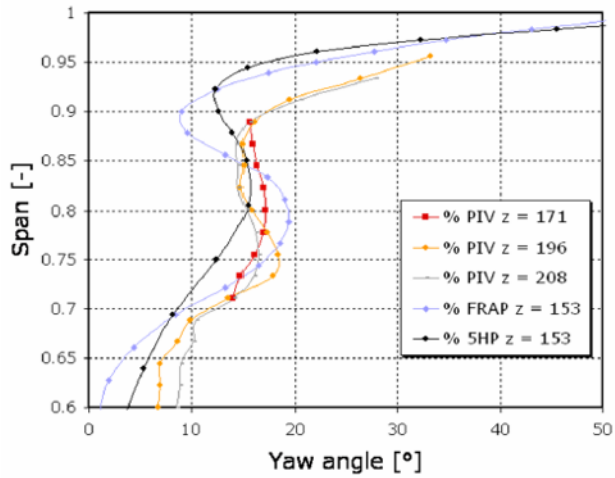


**Fig. 8.** Comparison between FRAP, 5HP and PIV time averaged pitchwise yaw angles – Turbine exit region

The PIV data have a shift in the lower section of the blade span. This behavior may be explained by taking into account that farther downstream of the blade row (up to z=208% tip axial chord) the leakage layer is more entrained in the main flow. It is interesting to note that FRAP and 5HP results are consistent throughout but the PIV results vary in comparison. The greatest variation is in the vicinity of the passage vortex core, where perhaps the errors in the out-of-plane velocity component in the PIV data contribute to the observed variation.

## 3 Results

Figure 9 shows the evolution of measured the tangential velocity at turbine exit region at one rotor blade position. The flow field is almost axial at the exit of the turbine stages and the tip passage vortex is identified in the middle of the measurement region with a higher tangential velocity.

Figure 10 shows contour plots at three blade span positions of the PIV measured yaw angle. Superimposed on the contour plots are vectors of the in-plane velocities. The contours in the middle of the measurement plane are blanked out as shown in the orange region with zero length vectors; these PIV data are unusable due to the optical distortion through the window. All the measurements are derived from phase locked data, that are averaged over 100 samples. At the 77% blade span plane, the measured yaw angle shows two distinct regions: the main "undisturbed" flow in the middle of the passage and the wake region that is close to the trailing edge. In the wake region the flow is underturned with yaw angles as large as 80°; the deficit in the axial velocity and the presence of the passage vortex causes this underturning. The wake region is highly confined, compared to the main flow, and thus there are large circumferential gradients in the yaw angle.

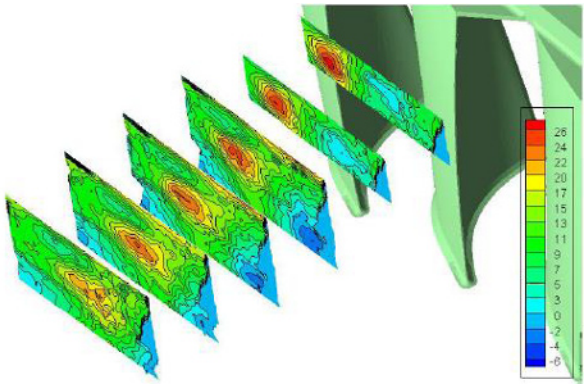

**Fig. 9.** Tangential velocity evolution – turbine exit region

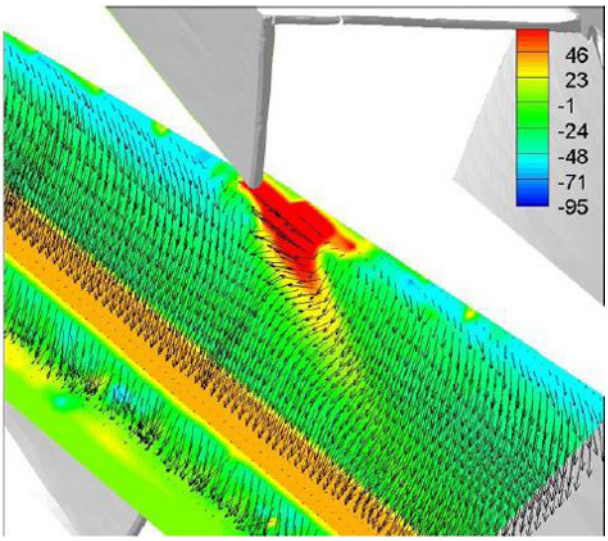


**Fig. 10.** PIV measured absolute yaw angles at different axial planes. Vectors show the in-plane velocity component – Interstage region 77% blade span

## 4 Conclusions

A stereoscopic PIV system has been successfully applied to measure the steady and unsteady flow field in the interstage region, turbine exit region and labyrinth path of a two-stage axial turbine. The application of such an optical measurement technique is quite rare in turbomachinery and the measured data are of great importance for further understanding of flow field dynamics.

To compensate for the optical distortion due to the curvature of the rotor casing, a calibration bench has been designed to allow a calibration on the entire measurement region.

A procedure has been developed in order to quantify the degree of uncertainty of the present measurements using artificially generated pictures and re-constructing the flow field using the same calibration procedure as in measurements. Error analysis shows that the in-plane velocity components (axial and tangential) are measured with an accuracy of +/- 2m/s while the radial velocity component can be assessed only qualitatively. These results are in agreement with other investigations. Moreover a comparison is done between PIV data and pneumatic and unsteady probe pressure data which show

good agreement and thus confirm the high quality of the data.

The applied 3D-PIV technique allowed measurements in a volume which can be related directly to pressure and velocity field. This unique set of data allows the possibility to improve flow modelling used in the design process and will be used furthermore to evaluate the loss mechanisms in the interstage region.

## References

1. M. P. Wernet, *Application of DPIV to study both steady state and transient turbomachinery flows,* Opt. Laser Technol. **32,** pp. 497-525 (2000).
2. N. Balzani, F. Scarano, M. L. Riethmuller, F. A. E. Breugelmans, *Experimental Investigation of the Blade-to-Blade in a Compressor Rotor by Digital Particle Image Velocimetry*, ASME J. Turbomach. 122, 743 (2000)
3. A. J. Sanders, J. Papalia, S. Fleeter, *MultiBlade Row Interactions in a Transonic Axial Compressor: Part I – Stator Particle Image Velocimetry (PIV) Investigation*, ASME J. Turbomach. **124** (2002)
4. O. Uzol, Y. C. Chow, J. Katz, C. Meneveau, *Experimental Investigation of Unsteady Flow Field Within a Two-Stage Axial Turbomachine Using Particle Image Velocimetry*, ASME J. Turbomach. **124** (2002)
5. B. Liu, H. Wang, H. Liu, H. Yu, H. Jiang, M. Chen, *Experimental Investigation of Unsteady Field in the Tip Region of an Axial Compressor Rotor Passage at Near Stall Condition with Stereoscopic Particle Image Velocimetry*, ASME J. Turbomach. **126**, 360 (2004)
6. E. Göttlich, J. Woisetschläger, P. Pieringer, B. Hampel, F. Heitmeir, *Investigation of Vortex Shedding and Wake-Wake Interaction in a Transonic Turbine Stage using LaserDoppler-Velocimetry and Particle Image Velocimetry*, ASME paper GT2005-68579.
7. W. J. Zang, A. K. Prasad, *Performance Evaluation of a Scheimpflug Stereocamera for Particle Image Velocimetry*, Appl. Opt., **36**, 8738-8744 (1997).
8. A. K. Prasad, *Stereoscopic Particle Image Velocimetry*, Exp. Fluids, **29**, pp. 103-116 (2000).
9. C. J. Kähler, B. Sammler, J. Kompenhans, *Generation and Control of Tracer Particles for Optical Flow Investigations in Air*, Exp. Fluids, **33**, pp. 736-742 (2002).
10. A. Mellin, *Tracer Particles and Seeding for Particle Image Velocimetry*, Meas. Sci. Technology **8,** pp. 1496-1416 (1997).
11. J. Westerweel, D. Dabiri, M. Gharib, *The Effect of a Discrete Window Offset on the Accuracy of Cross-Correlation Analysis of Digital PIV Recordings*, Exp. Fluids, **23**, pp. 20-28 (1997)
12. F. Scarano, M. L. Riethmuller, *Iterative Multigrid Approach in PIV Image Processing with Discrete Window Offset*, Exp. Fluids, **26**, pp. 513-523 (1999).
13. J. Westerweel, *Efficient Detection of Spurious Vectors in Particle Image Velocimetry*, Exp. Fluids, **16**, pp. 237-24 (1994).
14. M. Raffel, C. Willert, J. Kompenhans, *Particle Image Velocimetry – A Practical Guide*, Berlin Springer (1998)
15. C. E. Willert, M. Gharib, *Digital particle image velocimetry*, Exp. Fluids, **10**, pp. 181-193
16. R. D. Keane, R. J. Adrian, *Theory of cross correlation analysis of PIV images*, Appl. Sci. Res., pp.191-215 (1992).